

Hierarchically designed injectable hydrogel from oxidized dextran, amino gelatin and 4-arm poly(ethylene glycol)-acrylate for tissue engineering application†

Xiaohua Geng,^{ab} Xiumei Mo,^{*ab} Linpeng Fan,^b Anlin Yin^b and Jun Fang^{ab}

Received 18th July 2012, Accepted 8th October 2012

DOI: 10.1039/c2jm34737g

Hydrogels are high in water content and have physical properties similar to native extracellular matrix (ECM), and thus they have been widely studied as three-dimensional (3D) tissue engineering scaffolds for cell culture. In this work, a two-step process was introduced to fabricate injectable hydrogel from oxidized dextran (ODex), amino gelatin (MGel) and 4-arm poly(ethylene glycol)-acrylate (4A-PEG-Acr) for cell encapsulation. A primary network was formed based on a Schiff based reaction between ODex and MGel, then a UV light-induced radical reaction of 4A-PEG-Acr was used to produce the independent secondary network. Both of the reactions were carried out under physiological conditions in the presence of living cells with no toxicity. The primary network depending on natural polymers could degrade rapidly to provide space and nutrition for encapsulated cells' growth, and the secondary network could provide long-term mechanical stability. The attachment and spreading of pre-osteoblasts (MC3T3-E1) on IPN hydrogels were observed by DEAD/LIVE kit staining. Furthermore, cell spreading and cell proliferation within IPN hydrogels were observed using confocal microscopy after phalloidin/DAPI staining. The results showed that the as-prepared interpenetrating polymer network (IPN) hydrogels possessed good mechanical properties, a controllable degradation rate and favorable biocompatibility. Therefore, the hierarchically designed hydrogel in this study could be a promising candidate for bone or cartilage tissue engineering applications.

1. Introduction

Tissue engineering aims to promote the biological and functional regeneration of damaged or diseased tissues by incorporating cells and bioactive molecules into a supporting material or scaffold. Therefore, an appropriate tissue engineering scaffold should not only permit cell attachment and promote cell growth, but should also be biocompatible, biodegradable, and mechanically strong to withstand the forces imposed *in vivo*.^{1,2}

Hydrogels are a kind of material that have gained widespread application as 3D tissue engineering scaffolds due to their high water content and physical properties similar to ECM.^{3,4} Furthermore, hydrogels can maintain the diffusion of nutrients and oxygen to growing cells through varying levels of porosity.⁵ Currently, forming hydrogels *in situ* has been identified as highly important for the development of an injectable therapy.^{6,7}

Injectable therapy is implemented by injecting precursor solutions which contain cells or drugs directly into the damaged site, and the solutions are then solidified and fixed *in situ*. Methods of triggering gelation of precursor solutions include photopolymerization,⁸ Schiff-based reaction,^{9,10} click reaction,^{11,12} Michael addition,^{13,14} self-assembly,^{15,16} thermosensitivity,¹⁷ enzymatically crosslinking,^{18,19} and pH-sensitivity.^{20,21}

The challenge for hydrogel use as a cell carrier is how to make the cells spread and proliferate well within the formed hydrogels. In the past few years, several methods have been successfully developed to control cell growth spatially and temporally within hydrogels. Anseth's group demonstrated that encapsulated cells spread efficiently by chemically modified cell-affinitive domains such as RGD on poly(ethylene glycol) (PEG) chains.²² They also demonstrated that encapsulated cells migrated through degrading channels formed by precisely controlling the gel crosslinking density of the photodegradable hydrogels.²³ Webb's group

^aState Key Laboratory for Modification of Chemical Fibers and Polymer Materials, College of Materials Science and Engineering, Donghua University, Shanghai 201620, China. E-mail: xmm@dhu.edu.cn; Tel: +86 021 67792653

^bBiomaterials and Tissue Engineering Lab, College of Chemistry, Chemical Engineering and Biotechnology, Donghua University, Shanghai 201620, China

† Electronic supplementary information (ESI) available: ¹H NMR spectra for ODex (Fig. SI-1) and 4A-PEG-Acr (Fig. SI-2); phase diagram of gelatin and MGel (Fig. SI-3) SEM photographs of PBS salt sediments on dry hydrogels (Fig. SI-4); behaviour of different solutions during the two-step crosslinking method (Fig. SI-5); tensile testing of P and P-D-G-2 hydrogels (Fig. SI-6); compress testing on control hydrogels (Table SI-1 and Fig. SI-7); cell density on the hydrogel surface (Fig. SI-8); further evidence for the degradation of hydrogels (Fig. SI-9) and 3D cell culture (Fig. SI-10).

engineered a semi-interpenetrating network composed of hyaluronic acid and poly(ethylene glycol) diacrylate. And even low levels of hyaluronic acid content helped fibroblasts to spread and proliferate three-dimensionally through cell-mediated enzymatic degradation of the hyaluronic acid.²⁴

Designing hydrogels in the interpenetrating polymer network (IPN) style is a simple and easily feasible route to improve cell spreading and proliferation inside hydrogels. IPN hydrogels are one type of hybrid hydrogel composed of two or more cross-linked polymers, where each polymer is either a physically or chemically crosslinked network which is independent of the other while being physically interlocked.²⁵ Natural materials such as collagen, hyaluronic acid, dextran, and gelatin are biocompatible and easy to degrade, while synthetic polymers always possess favorable mechanical properties. Thus, it was hypothesized that by sequentially crosslinking natural and synthetic polymers, a hybrid hydrogel with good cyto-compatibility and tunable mechanical properties could be yielded.

To test the hypothesis, we developed and evaluated an *in situ* forming hydrogel composed of natural and synthetic polymers. Specifically, dextran is a natural biodegradable polysaccharide chemically similar to glycosaminoglycans (an important constituent of ECM).²⁶ More importantly, the abundant pendant hydroxyl groups on the polysaccharide chains enable it to be chemically modified.^{27,28} Gelatin is a denatured product of collagen which has been proven to have good biocompatibility *in vivo*. Additionally, gelatin retains cell-binding motifs such as RGD, which is critical for cell culture in a 3D environment.^{29,30} Currently, PEG is favored in biomedical scaffold fabrication due to its bioinert nature and easily controllable mechanical properties.^{31,32} Here, dextran was oxidized with sodium periodate to acquire aldehyde groups, and ethane diamine was used to chemically modify the carboxyl groups on gelatin chains to amino groups. Then, a Schiff based reaction between the aldehyde groups and the amino groups crosslinked the ODex and MGel to form the primary network. Sequentially, 4-arm-poly(ethylene glycol) (4A-PEG) was functionalized with acrylate groups which allow radical photopolymerization under light irradiation to form the secondary network.

The swelling, degradation, rheological, and mechanical properties of IPN hydrogels were evaluated. Adhesion and spreading of cells on the hydrogel surface were observed. Furthermore, the viability, spreading, and proliferation of MC3T3-E1 cells encapsulated in different IPN hydrogels were tracked. The results demonstrated that IPN hydrogels had favorable physical

and biological properties, and therefore could be a promising scaffold for tissue engineering application.

2. Materials and methods

2.1 Materials

4A-PEG (M_w 20 000) was obtained from Jemyork Biotechnology Co. Ltd, Shanghai, China. Triethylamine (TEA), dichloromethane (DCM), acryloyl chloride, diethyl ether, 1-[4-(2-hydroxyethoxy)-phenyl]-2-hydroxy-2-methyl-1-propane-1-one (I2959), dextran (M_w 100 000), sodium periodate, ethane diamine (ED), gelatin (type B, M_w 60 000), phosphate buffer saline (PBS, pH = 7.4), and dimethyl sulfoxide (DMSO) were purchased from Sigma-Aldrich, and used as received. 1-Ethyl-3-(3-dimethyl aminopropyl) carbodiimide hydrochloride (EDC) was supplied by GL Biochem (Shanghai, China). Dialysis tube (MWCO 3500 and 1000) was obtained from JingKeHongDa Biotechnology Co., (Shanghai, China). All other chemicals, unless specified otherwise, were from Sigma-Aldrich.

MC3T3-E1 cells were obtained from the institute of Biochemistry and Cell biology (Chinese Academy of Sciences, China). Fetal bovine serum (FBS), methylthiazol tetrazolium (MTT), penicillin–streptomycin (Pen–Strep) solution and all other culture media were purchased from Gibco. Tissue culture polystyrene flasks were obtained from Corning, Co., China. LIVE/DEAD Viability/Cytotoxicity Assay Kit, phalloidin-Alexa568, and DAPI were purchased from Invitrogen, USA.

2.2 Synthesis and characterization of ODex and MGel

As shown in Fig. 1a, ODex was prepared by using sodium periodate to oxidize the dextran. Specifically, 6.34 g of NaIO_4 (dissolved in 100 ml of distilled water) was added dropwise to 100 ml of dextran solution (10 wt%), the solution was stirred for 6 hours at room temperature and shielded from light. Then, 2 ml of ethylene glycol was added to terminate the reaction. Lastly, the ODex solution was dialyzed exhaustively (MWCO 3500) for 3 days against water, and lyophilized to obtain the final product (yield: 70%).

The oxidation degree of ODex was determined by quantifying the aldehyde groups formed by *tert*-butyl carbazate *via* carbazone.^{9,10} Briefly, an ODex solution (1 wt% in pH = 5.2 acetate buffer) was prepared, and fivefold excess of *tert*-butyl carbazate in the same buffer was added and the mixtures allowed to react for 24 h at room temperature followed by addition of a fivefold

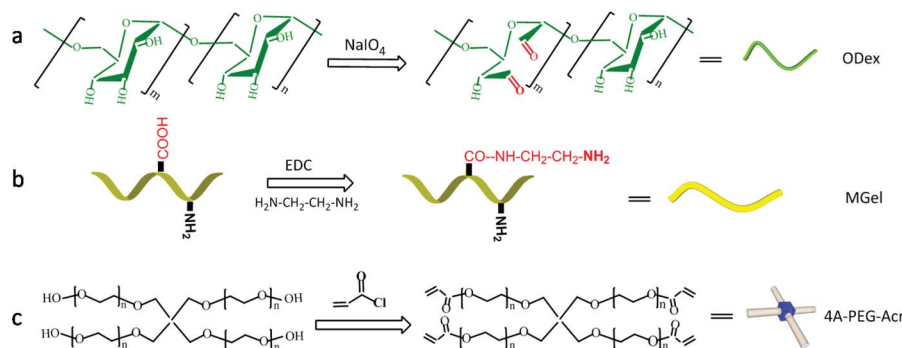


Fig. 1 Synthesis of ODex (a), MGel (b) and 4A-PEG-Acr (c).

excess of NaBH_3CN . After another 12 h, the reaction product was precipitated thrice with acetone and the final precipitate was dialyzed against water for three days, then the solution was lyophilized. The actual degree of oxidation was assessed by ^1H NMR (ESI, Fig. SI-1†) by integrating the peak at 1.3 ppm (*tert*-butyl) against 4.8 ppm (anomeric proton of dextran).

MGel was prepared according to our previously described method with some changes (Fig. 1b).³³ Specifically, 5 g of gelatin was dissolved in 100 ml of sodium dihydrogen phosphate buffer (pH = 5.0). Then, 16 ml of ethane diamine was added. After that the pH value was titrated back to 5 using hydrochloric acid (HCl) and 2.3 g of EDC was then added. The final molar ratio of carboxyl groups on the gelatin chains, EDC, and ethane diamine was 1 : 2 : 40. The reaction was stirred overnight at room temperature. Hereafter, the resulting mixture was dialyzed (MWCO 3500) against distilled water to remove the excess ethane diamine. The final dry products were obtained by freeze-drying with a yield of 85%.

The vial-inverting approach was used to determine the sol-gel transition temperature of gelatin and MGel solutions. Each sample with a given concentration was stored in vials at 4 °C. Then the vials with polymer hydrogels were immersed in a water bath, and the samples were regarded as a “gel” in the case of no visual flow within 30 s by inverting the vial with a temperature increment of 1 °C per step.³⁴

The amino group content in MGel was determined by the method we described previously.³³ Briefly, 0.5 ml of 0.0625 mg ml^{-1} MGel aqueous solution was mixed with 0.5 ml of PBS, 1.0 ml of 4 wt% sodium bicarbonate, and 1.0 ml of 0.1 wt% 2,4,6-trinitrobenzene-sulfonic acid sodium salt in water. After incubation at 37 °C for 2 h, the optical density of the solution was determined at 420 nm using a Hitachi UN-2500 spectrometer. The result was converted into free amino content (mmol g^{-1}) using a calibration curve obtained with β -alanine solutions as a standard.

2.3 Synthesis and characterization of 4A-PEG-Acr

4A-PEG-Acr was synthesized from 4A-PEG according to the procedure described elsewhere with minor modifications (Fig. 1c).^{35,36} Typically, 8 g of 4A-PEG (0.8 mmol) were dissolved in 200 ml of anhydrous DCM followed by azeotropic distillation in order to remove the trace water in this system.

Then the flask was cooled down to room temperature and TEA was added, followed by acryloyl chloride in DCM added dropwise to the flask. The final molar ratio of 4A-PEG, acryloyl chloride, and TEA was 1 : 8 : 8. The reaction was allowed to proceed at room temperature under a nitrogen atmosphere for 24 hours. Subsequently, the insoluble salt (triethylamine-HCl) was filtered, and the polymer solution was precipitated in cold diethyl ether. The precipitate was further purified by dialysis (MWCO 1000) for one day to remove unreacted starting materials and other byproducts. Finally, it was frozen at -20 °C and lyophilized to obtain the 4A-PEG-Acr. The final yield was approximately 65%.

The chemical structure of 4A-PEG-Acr was confirmed by using a FTIR spectrophotometer (NEXUS-670). Substitution of 4A-PEG-Acr was determined by ^1H NMR (Bruker Avance 400 MHz) spectrum by integrating the peak at 6.1 ppm (CH_2CH_2) against 5.8 ppm and 6.4 ppm (CHCH_2) (Fig. SI-2†).

2.4 Hydrogel formation

The preparation of IPN hydrogels is illustrated in Fig. 2. Briefly, ODex, MGel, and 4A-PEG-Acr solutions in PBS, and I2959 solution (dissolved in DMSO) were added into a tube. After homogenizing, the pre-polymer solutions were injected into 48-well culture plates. Then, they were incubated at 37 °C for 15 min, during which the primary crosslinking network was formed *via* the Schiff based reaction between ODex and MGel. This was followed by exposure of the formed hydrogels to 5 mW cm^{-2} UV light (365 nm) for 5 min to allow free radical polymerization of the 4A-PEG-Acr to form the secondary crosslinking network. The IPN hydrogel was formed by this two step crosslinking.

IPN hydrogels were prepared with a final 4A-PEG-Acr concentration of 55 mg ml^{-1} (P-D-G-1) and 40 mg ml^{-1} (P-D-G-2), respectively (Table 1), and the concentrations of ODex and MGel for both were 30 mg ml^{-1} and 50 mg ml^{-1} , respectively. For the control groups, P hydrogels were prepared with pure 4A-PEG-Acr with a concentration of 55 mg ml^{-1} , while D-G hydrogels were prepared with pure ODex and MGel at a concentration of 30 mg ml^{-1} and 50 mg ml^{-1} , respectively. Photoinitiator (I2959) was added to all the groups to a final concentration of 0.1 wt%. I2959 was chosen due to its aqueous solubility and good cytocompatibility.³⁷

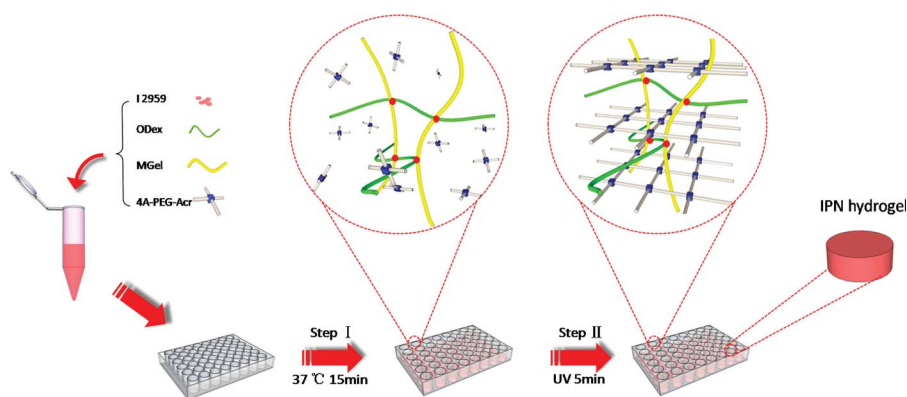


Fig. 2 Schematic for preparation of ODex–MGel–4A-PEG-Acr IPN hydrogels. IPN hydrogels were formed through a Schiff-based reaction (step I) and UV crosslinking (step II) in the presence of photoinitiator (I2959).

Table 1 Composition of the hydrogels

Sample	Concentrations (mg ml ⁻¹)			Total
	4A-PEG-Acr	ODex	Gelatin	
P	55	0	0	55
P-D-G-1	55	30	50	135
P-D-G-2	40	30	50	120
D-G	0	30	50	80

2.5 Swelling and degradation

The swelling test of the hydrogels was performed according to the protocol introduced elsewhere.³⁸ Briefly, cylindrical hydrogels (Ø 10 mm × 2 mm) were prepared as described above and immersed in PBS at 37 °C for overnight to reach a swelling equilibrium. Then, the swollen hydrogels were removed. After wiping off the surface water, the swollen weight of the hydrogels was recorded as (W_s). Then, the hydrogels were frozen and lyophilized to obtain the dry weight (W_d). The swelling ratio (Q_o) was calculated by eqn (1):

$$Q_o = (W_s - W_d)/W_d \quad (1)$$

To characterize the degradation properties of the hydrogels, the hydrogel samples were incubated in PBS solutions with NaN₃ (0.02 wt%) at 37 °C. At a predefined time, the samples were removed, frozen, and lyophilized. The weight remaining was calculated by using eqn (2):

$$\text{Weight remaining \%} = W_i/W_f \times 100\% \quad (2)$$

where W_i is the initial dry weight of the sample and W_f is the final dry weight of the sample. The swelling and degradation experiments were conducted in triplicate.

2.6 Rheological and vial tilting characterization

To characterize the real-time change of the hydrogel mechanical properties with crosslinking, the G' (storage modulus) and G'' (loss modulus) were monitored *via* dynamic oscillatory shear rheometry at 1% strain and 1 Hz using a Haake RS 150L Rheometer (Thermo Haake Co., Germany). All tests were performed at a constant temperature of 37 °C with parallel plate geometry (diameter = 25 mm). Specifically, the pre-polymer solution was mixed and pipetted directly onto the bottom plate, and the top plate was lowered to contact the gelling solution with a 2 mm gap size. The evolution of the G' and G'' was monitored with time. The hydrogel was allowed to undergo crosslinking for 15 min, then the gel was irradiated by 365 nm UV light through the gap to verify the possible change of elastic modulus caused by photopolymerization.

Vial tilting was used to visually characterize the sol–gel transition during the hydrogels' preparation. Vial tilting was performed after each crosslinking step, and 10 ml beakers were used in our experiment.

2.7 Compressive mechanical test

The mechanical properties of the hydrogels were measured by compression tests with a Dejie DXLL-20000 materials testing

instrument at room temperature. Briefly, cylindrical hydrogels (Ø 10 mm × 4 mm) were prepared as described above and immersed in PBS at 37 °C for overnight to reach a swelling equilibrium. After the diameter and thickness of the hydrogels were recorded, they were put on the lower plate and compressed by the upper plate at a strain rate of 1 mm min⁻¹. The Young's modulus (E) was calculated as the slope of the stress–strain curve, in the range of strain from 0 to 10%. All samples were analyzed in triplicate.

2.8 MC3T3-E1 cell culture

MC3T3-E1 cells were expanded and passaged at standard culture conditions in α -MEM medium (Gibco, USA) supplemented by 10% fetal bovine serum, and 1% penicillin/streptomycin. The complete medium was replaced every other day. All the cells before a passage number of 10 were used in this study.

2.9 Adhesion and spreading of MC3T3-E1 cells on hydrogels

To investigate the cell behavior (adhesion and spread) on IPN hydrogels, MC3T3-E1 cells were seeded at a density of 1×10^4 cells cm⁻² on the surface of the hydrogels fabricated as described in Section 2.4. The culture medium was changed every day. After 2 days of *in vitro* culture, the medium was discharged and the hydrogels were washed with PBS, then LIVE/DEAD Viability/Cytotoxicity Assay Kit solution containing 2 μ M calcein acetoxyethyl (AM) and 4 μ M ethidium homodimer (EthD-III) was added and incubated at 37 °C for 10 min. The stained cells were visualized with a fluorescent microscope (UL100HG Olympus Corporation, Japan). ImageJ software was used to quantify cell number from the fluorescence images. At least four images from four samples for each group were used for quantification of the cell number.

2.10 Spreading and proliferation of encapsulated cells in 3D culture

For cell encapsulation, MC3T3-E1 cells were premixed with pre-polymer solutions at a density of 5×10^6 cells ml⁻¹. The mixture was injected into 48-well culture plates, where the cells were encapsulated in hydrogels by the two-step crosslinking process as mentioned above. Then, complete medium was added on top of the hydrogel disks, followed by incubation under standard culture conditions with the medium exchanged every other day.

The cell viability in the hydrogels was quantified using the MTT assay for 4 and 8 days, following the method described elsewhere.³⁹ Briefly, MC3T3-E1 cells were incubated with 0.5 mg ml⁻¹ MTT at 37 °C and 5% CO₂ for 4 h. The solutions were then removed followed by addition of DMSO. After that, the hydrogels were left in the incubator for an additional 10 hours to ensure the diffusion of purple formazan salts, and finally the absorbance of the resulting solution was measured at 492 nm using a multidetection microplate reader (MK3, Thermo, USA). Three parallels were averaged for each specimen.

Laser scanning confocal microscope (Carl Zeiss LSM 700, Jena, Germany) was used for cell morphology observation. Immunostaining was performed according to the protocols introduced by the literature.³⁹ In brief, at a specific time interval, MC3T3-E1 cells were fixed using 4% formaldehyde for more

than 30 min, then incubated in 0.25% Triton X-100 for 1 h. After this step, MC3T3-E1 cells were stained overnight with phalloidin-Alexa568. Then the cells were counter stained with DAPI. All staining steps were performed at 4 °C, and two 30 min washes in PBS (pH = 7.4) were performed between each step to ensure the diffusion of the molecules in and out the specimens. In order to obtain the 3D distribution and spreading morphology of the encapsulated cells, a stack of images was acquired in the *z* dimension of successive slices with a thickness of 8 μm in each.

2.11 Statistical analysis

Statistical significance was determined using one-way ANOVA (analysis of variance) followed by Bonferroni's Multiple Comparison Test. Statistical significance was set to a *P* value <0.05. All data are presented as the mean values, and the error bars represent the standard deviation.

3. Results and discussion

3.1 Characterization of ODex and MGel

Dextran contains vicinal hydroxyl groups that can be readily modified with periodate to form aldehyde groups. The oxidized dextran bearing aldehyde groups serves as a good macromolecular crosslinker for polymers with amino groups. In this study, the actual oxidation of dextran was determined as approximately 41% by ¹H NMR.

In general, gelatin maintains a gel or viscous state under room temperature, which is unfavourable for injectable applications. Here, through reacting with ethane diamine, carboxyl groups on gelatin chains were chemically modified to amino groups. Therefore, the strong hydrogen bonds between amino and carboxyl groups, which mainly lead to the gel state of gelatin, could be disrupted.³³ As a result, an MGel solution with a high concentration could maintain its liquid state at room temperature (as shown in Fig. SI-3†). The amino content of MGel was determined as approximately 0.802 mmol g⁻¹ by the TNBS method.

3.2 Characterization of 4A-PEG-Acr

4A-PEG-Acr was synthesized *via* terminal modification of 4A-PEG with acryloyl chloride. As shown in Fig. 3, the absorption

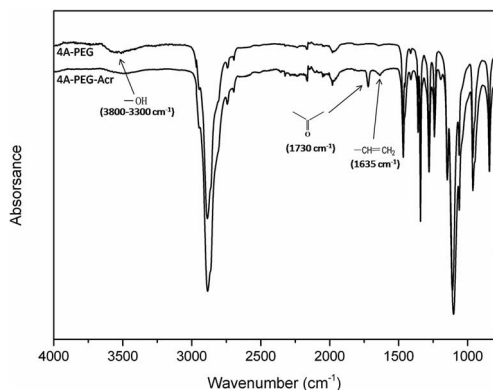


Fig. 3 IR spectra of 4A-PEG and 4A-PEG-Acr.

bands at 1730 cm⁻¹ and 1635 cm⁻¹ were attributed to ester carbonyl (C=O) and vinyl (-CH=CH₂) groups, respectively.⁴⁰ And the broad peak appearing at 3800–3300 cm⁻¹ was attributed to terminal hydroxyl groups on 4A-PEG. The decline of the hydroxyl groups, as well as the appearance of ester carbonyl and vinyl groups confirmed the acylation of 4A-PEG and the formation of 4A-PEG-Acr. The substitution degree of 4A-PEG was determined as approximately 91% by ¹H NMR.

3.3 Swelling and degradation properties

Fig. 4 shows that all four hydrogels contained significant amounts of water, as reflected by their equilibrium swelling ratios of 20 to 30. The swelling ratio for control groups (P, and D-G) was higher than that of the IPN hydrogels. For P and D-G hydrogels, the swelling ratio was 24.63 and 29.57, respectively. As for the IPN hydrogels, the swelling ratio decreased to 20.73 (P-D-G-1) and 21.90 (P-D-G-2), respectively.

The equilibrium swelling ratio is generally influenced by the crosslinking density, gel composition, *etc.*⁴¹ Among all the hydrogels, two IPN hydrogels showed the lowest swelling ratio due to the existence of two crosslinking networks which gave the highest crosslinking density. Of the two IPN hydrogels, P-D-G-1 had a higher 4A-PEG-Acr content, and therefore had a higher crosslinking density which caused a lower swelling ratio. Since there was only one network in the 4A-PEG-Acr hydrogel which gave a low crosslinking density, it had a higher swelling ratio than IPN hydrogels. D-G hydrogels also had only one crosslinking network whilst the network based on Schiff based crosslinking showed weak intensity compared with radical photopolymerization crosslinking; therefore, D-G hydrogels gave the highest swelling ratio.

Fig. 5 shows the degradation profiles of the different hydrogels. Disparate performance on degradation has been shown among the four hydrogels. D-G hydrogel lost its weight quickly, and dissolved totally at day 7. This can be ascribed to the weak crosslinking state induced by the Schiff based reaction. Besides, as shown in Fig. 4, the highest swelling ratio was also one of the reasons for the fast disintegration of the D-G hydrogel. Conversely, hydrogels composed of pure 4A-PEG-Acr only lost 10% of their original weight in 21 days degradation, which indicated that 4A-PEG-Acr hydrogel was very stable when incubated in PBS. Interestingly, by combine the two components to make an IPN hydrogel, controllable degradation properties

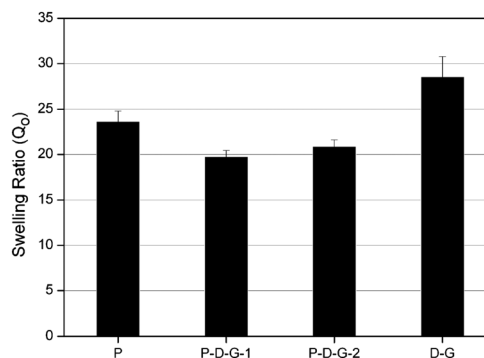


Fig. 4 Swelling ratio of hydrogels incubated in PBS at 37 °C.

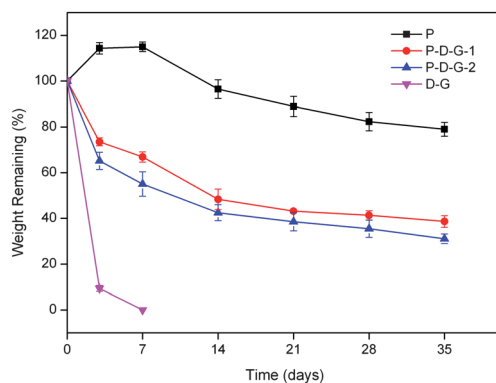


Fig. 5 Degradation of hydrogels in PBS at 37 °C with respect to weight loss.

can be obtained. As shown in Fig. 5, the degradation rate of IPN hydrogels was relatively fast during the initial two weeks and almost lost half their original weight after two weeks. This can be ascribed to the disintegration of the primary crosslinking network which was formed of ODex and MGel. Then the degradation rate slowed down due to the existence of the bioinert 4A-PEG-Acr crosslinking network. It is worth noting that the degradation curve of P exhibited an increase in behavior instead of a decrease during the initial several days. This can be ascribed to the deposition of PBS salt in the hydrogels when they were immersed in PBS solutions (see Fig. SI-4†) which induced the dry weight of 4A-PEG-Acr hydrogels to increase slightly.

One of the goals of tissue engineering is to ensure that tissue constructs can be incorporated into the surrounding host tissue. In respect of degradation, a mismatch of the degradation rate of the scaffold and the growth rate of new tissue can lead to premature failure of tissue development.⁴² This requires the biopolymer scaffolds to possess an optimal degradation rate. In our study, the IPN hydrogels were composed of natural materials and synthetic polymer. Through altering the content ratio between the two components, adjustable degradation properties can be obtained. Furthermore, due to the existence of 4A-PEG-Acr, our IPN hydrogels can last for a long period without being physically disintegrated, which is particularly useful for bone and cartilage tissue engineering.^{43,44}

3.4 Rheological analyses

A two-step protocol was used to synthesize IPN hydrogels. Fig. 6 shows the time sweep profiles of G' and G'' for the P-D-G-2 hydrogel forming. As shown in Fig. 6a, initially, G'' is larger than G' , which was expected since the samples were still in a liquid state where viscous properties dominate. With the occurrence of Schiff based reaction, the solutions began to gel, and both G' and G'' begin to increase. However, the rate of increase of G' was much higher than that of G'' . As a consequence, there was a crossover point where G' becomes larger than G'' . The time required for this crossover to occur was referred to as the gelation time and this point was referred to as the gelation point.⁴⁵ After the gelation point, the elastic properties began to dominate. For the P-D-G-2 hydrogel, the gelation time was approximately 58 seconds. After 15 min, UV light was introduced to start the

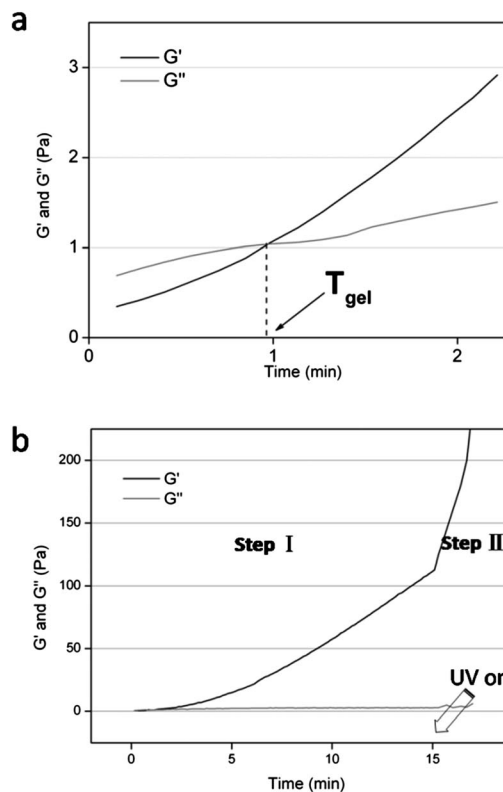


Fig. 6 Representative evolution of shear storage modulus (G') and shear loss modulus (G'') as a function of time during the primary gelation (a) and secondary gelation (b) of P-D-G-2 hydrogels.

secondary crosslinking in IPN hydrogels (Fig. 6b), and the rapid increase of G' demonstrated the occurrence of radical photopolymerization between the 4A-PEG-Acr chains.

Fig. SI-5† shows the photographs taken during the vial tilting test. After the first crosslinking step induced by the Schiff based reaction, P-D-G-1, P-D-G-2, and D-G samples all became immobile (Fig. SI-5f–h†). However, P group (Fig. SI-5e†) did not become solid because there is only 4A-PEG-Acr component exist in this group. After the UV induced photocrosslinking, all the groups became immobile (Fig. SI-5i–l†), which indicated that the second crosslinking step had happened.

3.5 Mechanical properties

Fig. 7 shows the typical compressive stress–strain curves of the hydrogels. The elastic modulus, fracture stress, and fracture strain of the hydrogels are summarized in Table 2. IPN hydrogels have shown significantly higher elastic moduli compared with that of D-G and P groups. For P-D-G-1 and P-D-G-2 hydrogels, the elastic moduli were 19.84 kPa and 32.27 kPa, respectively. Meanwhile, the elastic moduli for D-G and P groups were only 3.05 kPa and 9.88 kPa, respectively. IPN hydrogels also possess apparently higher fracture stress compared with that of pure 4A-PEG-Acr hydrogel or ODex–MGel hydrogel. According to Table 2, the fracture stresses for P-D-G-1 and P-D-G-2 hydrogels were 76.97 kPa and 90.70 kPa, respectively, which were higher than that of P hydrogel (50.40 kPa) and significantly higher than that of D-G hydrogel (16.28 kPa). Additionally, although with

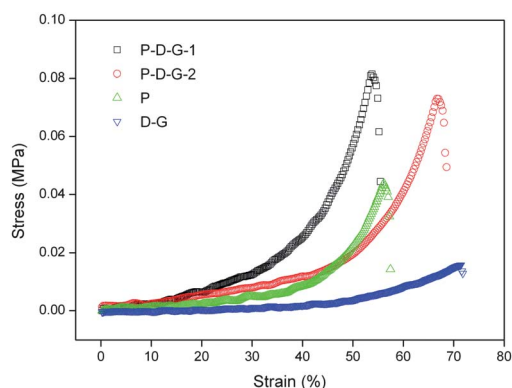


Fig. 7 Representative stress–strain curves of P, P-D-G-1, P-D-G-2, and D-G hydrogels at room temperature.

Table 2 Compression properties of hydrogels at room temperature^a

Samples	<i>E</i> (kPa)	Fracture stress (kPa)	Fracture strain (kPa)
D-G	3.05 ± 1.17	16.28 ± 2.61	72.21 ± 2.88
P	9.88 ± 2.40	50.40 ± 3.15 ^b	55.01 ± 2.65 ^b
P-D-G-2	19.84 ± 4.16 ^{b,c}	76.97 ± 6.20 ^{b,c}	69.90 ± 3.21 ^{c,d}
P-D-G-1	32.27 ± 2.66 ^{b,c,d}	90.70 ± 6.61 ^{b,c}	56.93 ± 3.57 ^{b,d}

^a Comparisons were made with pairs with statistical analysis by using one-way ANOVA followed by Bonferroni's Multiple Comparison Test at level of $P < 0.05$. ^b Significantly different from that of D-G hydrogel. ^c Significantly different from that of P hydrogel. ^d Significantly different from that of P-D-G-1 hydrogel ($n = 3$).

the same content of 4A-PEG-Acr, the fracture strain of P-D-G-2 hydrogel (69.90%) was also higher than that of P hydrogel (55.01%). Furthermore, tensile testing of the hydrogels can be obtained through ESI, Fig. SI-6.† As illustrated, P hydrogel became fractured when it was stretched to approximately double its original length. However, P-D-G-2 hydrogel can still maintain elasticity at the state of double elongation.

In order to explain the improvement in mechanical properties for IPN hydrogels, two reasons can be taken into consideration. First, by combining the ODex–MGel network, the tough but fragile PEG-Acr chains can glide through the ODex or MGel chains. With the crack energy dissipation to the ODex–MGel networks, IPN hydrogels can obtain an enhancement of fracture stress and fracture strain. Secondly, as mentioned for the swelling test, the equilibrium swelling ratio of IPN hydrogels was also smaller than that of pure 4A-PEG-Acr hydrogel. Thus, the relatively higher equilibrium polymer content was also a considerable advantage that enables the IPN hydrogels to resist higher stress.

To confirm that IPN hydrogels have preferable mechanical properties compared with pure 4A-PEG-Acr hydrogels or ODex–MGel hydrogels, three kinds of hydrogels were prepared with the same polymer content of 120 mg ml⁻¹ which are illustrated in Table SI-1.† The stress–strain curves of the three hydrogels are shown in Fig. SI-7.† Although P' hydrogel had a higher elastic modulus and fracture stress, the apparent defect in fracture strain indicated that the P' hydrogel was more fragile than the other hydrogels. Conversely, the P-D-G-2 hydrogels demonstrated both considerable fracture stress and the highest fracture strain among the three hydrogels, while the D-G' hydrogels gave the lowest fracture stress among the three hydrogels.

Since many load-bearing tissues such as cartilage, tendon, bone, and muscle need to frequently exhibit high strength and toughness, thus, tissue engineering scaffolds tend to be applied in these fields needing to possess considerable mechanical strength. In this study, mechanically strong IPN hydrogels were prepared by combining two independent networks, which have overcome both the weak elastic modulus of the ODex–MGel network and the fragile property of the 4A-PEG-Acr network. Therefore, the IPN hydrogels could be promising matrixes for load-bearing tissue engineering.

3.6 MC3T3-E1 cells adhesion and spread on the surface of hydrogels

Fig. 8 shows MC3T3-E1 cells spread on the surface of P and P-D-G-2 hydrogels after being cultured *in vitro* for 2 days. It can be seen that there were few cells on the P hydrogel, and the cells had a round shape (Fig. 8a). This observation is in good agreement with previously published data which suggested that PEG resisted cells adhering due to its highly hydrophilic and low protein absorption properties.^{46,47} However, by incorporation of MGel and ODex which could provide more cell adhesion sites, there were many more cells adhering to the surface of the IPN hydrogel and the cells had a spindle shape (Fig. 8b). Additionally, almost all of the adherent cells on the IPN hydrogel stayed alive after 2 days of culture (cells in green color represent live cells, and those in red color represent dead cells), which demonstrated that the

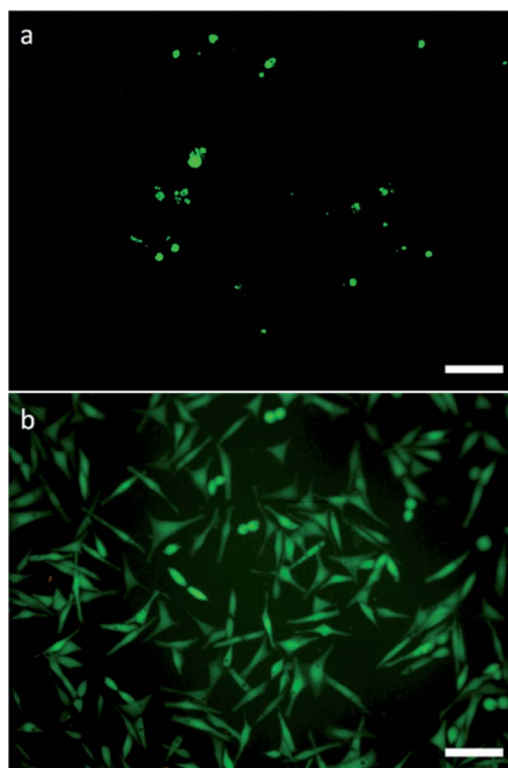


Fig. 8 MC3T3-E1 cell adhesion and spreading on the surface of P (a) and P-D-G-2 (b) hydrogels after 2 days culture. A pure 4A-PEG-Acr hydrogel does not promote cell adhesion (little cell adhesion visible), while an IPN hydrogel that contained ODex and MGel can significantly enhance cell adhesion and spreading. Scale bar represents 100 μm.

IPN hydrogels can provide a favorable two dimensional (2D) environment for MC3T3-E1 cells to adhere and spread without showing apparent toxicity.

Since the ability of cells to attach and spread on hydrogels is an important attribute for tissue development,³⁸ the cell density on different hydrogels was analysed. As shown in Fig. SI-8,† after 2 days culture, the cell density on the surface of P-D-G-2 hydrogel was statistically higher than that on P hydrogel. For P-D-G-1 group, it is supposed that the higher content of 4A-PEG-Acr was unfavorable for cell adhesion. For D-G groups, the relatively soft mechanical properties were also less favorable for cell attachment which has been discussed in previous research.⁴⁸

3.7 Viability and long-term proliferation of encapsulated MC3T3-E1 cells

The MTT assay was implemented to quantitatively investigate the metabolic activity of MC3T3-E1 cells within hydrogels. The more cells present, the higher the optical density (O.D.) that can be detected. As shown in Fig. 9, after 4 days of culture, cells within IPN hydrogels showed statistically higher metabolic activity than cells in P hydrogel. Notably, the D-G group showed a remarkably higher O.D. value than that of all the other groups on day 4, which demonstrated that the ODex-MGel hydrogel network can provide an excellent environment for cells to grow in. However, on day 8, due to the collapse of the ODex-MGel hydrogels caused by the rapid degradation of the ODex-MGel network, the hydrogels had been disintegrated (Fig. 5). Therefore, cells within the hydrogel could be taken away during MTT test, resulting in a dramatically decreased O.D. of the D-G group. In contrast, cell metabolic activity in IPN hydrogels increased statistically as culture time increased. On day 8, both P-D-G-1 and P-D-G-2 hydrogels showed higher cell metabolic activity than that seen on day 4. However, the O.D. of P hydrogels on day 8 was less than that on day 4, which demonstrates that the pure 4A-PEG-Acr hydrogel is unfavorable for long-term 3D cell culture.

Fig. 10 shows the fluorescence micrographs of cell-laden hydrogels. After 4 days of culture *in vitro*, most of the cells within P hydrogel were round (Fig. 10a), while within IPN hydrogels, some of the cells had started to form extensions, indicating that

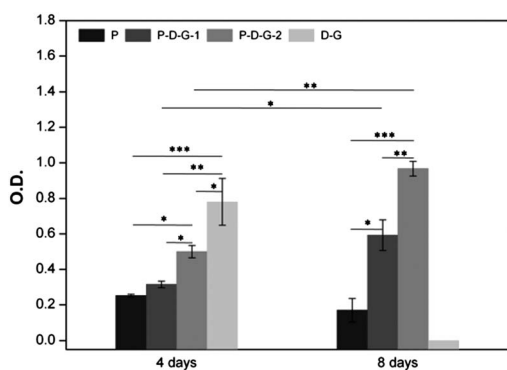


Fig. 9 MTT analysis of MC3T3-E1 cells after encapsulation in hydrogels for 4 and 8 days. For IPN hydrogels, cell metabolic activity was statistically higher at day 8 than at day 4. * $P < 0.05$, ** $P < 0.001$, and *** $P < 0.0001$ ($n = 3$).

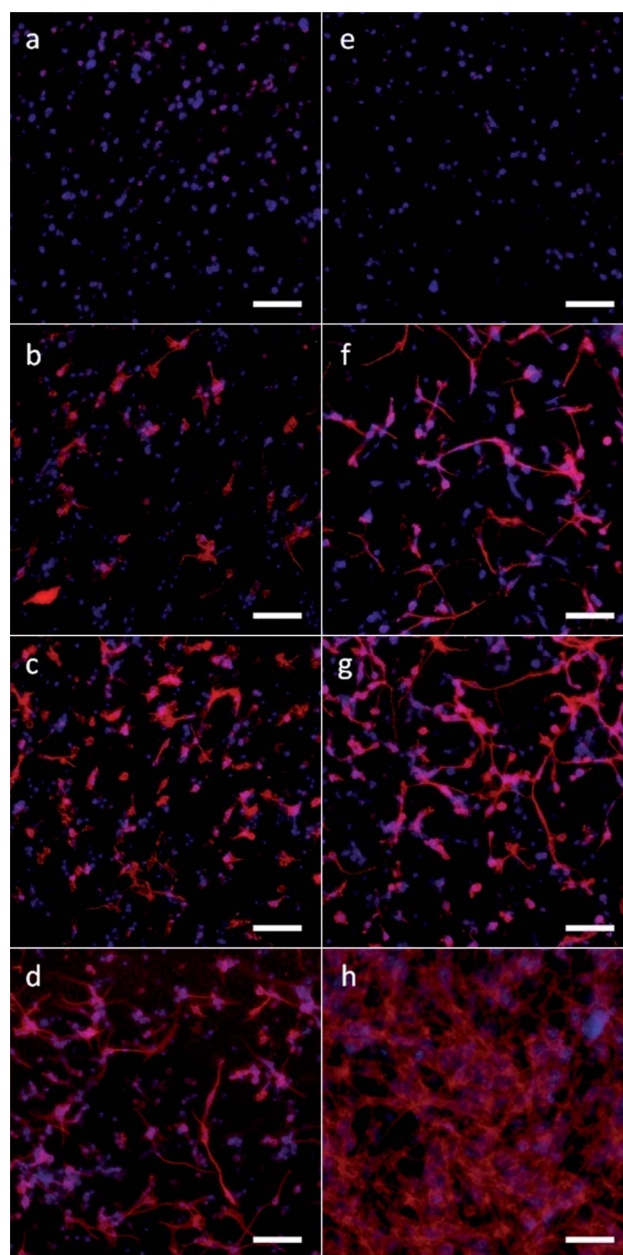


Fig. 10 Fluorescence micrographs of MC3T3-E1 cells encapsulated within P, P-D-G-1, P-D-G-2, and D-G hydrogels by day 4 (a, b, c, and d, respectively), and day 8 (e, f, g, and h, respectively). The cytoplasm was stained by phalloidin-Alexa568, and the nucleus was stained by DAPI. Scale bar represents 100 μm . Cell seeding density is 5×10^6 cells ml^{-1} .

the cells were starting to spread (Fig. 10b and c). In D-G hydrogel, cells in a spindle shape had already spread (Fig. 10d). By 8 days of culture, many of the cells in P-D-G-1 (Fig. 10f) and P-D-G-2 (Fig. 10g) hydrogels were in a spindle shape, whereas in P hydrogel (Fig. 10e), most cells were still round and no cells had developed extensions. The results corresponded well with the MTT assays as mentioned above. After 8 days of culture, the D-G hydrogel had disintegrated (data not shown), and cells within the hydrogel had moved out from the bulk of the hydrogel and proliferated on the surface of tissue culture polystyrene (Fig. 10h).

Fig. 11 shows the 3D distribution of MC3T3-E1 cells encapsulated in P hydrogel (Fig. 11a), P-D-G-2 hydrogel (Fig. 11b), and D-G hydrogel (Fig. 11c) after 4 days of culture. As illustrated, cells had a wide distribution in height (indicated by color differences of cells) among P hydrogel and P-D-G-2 hydrogel on day 4. In contrast, the single color distribution in the D-G

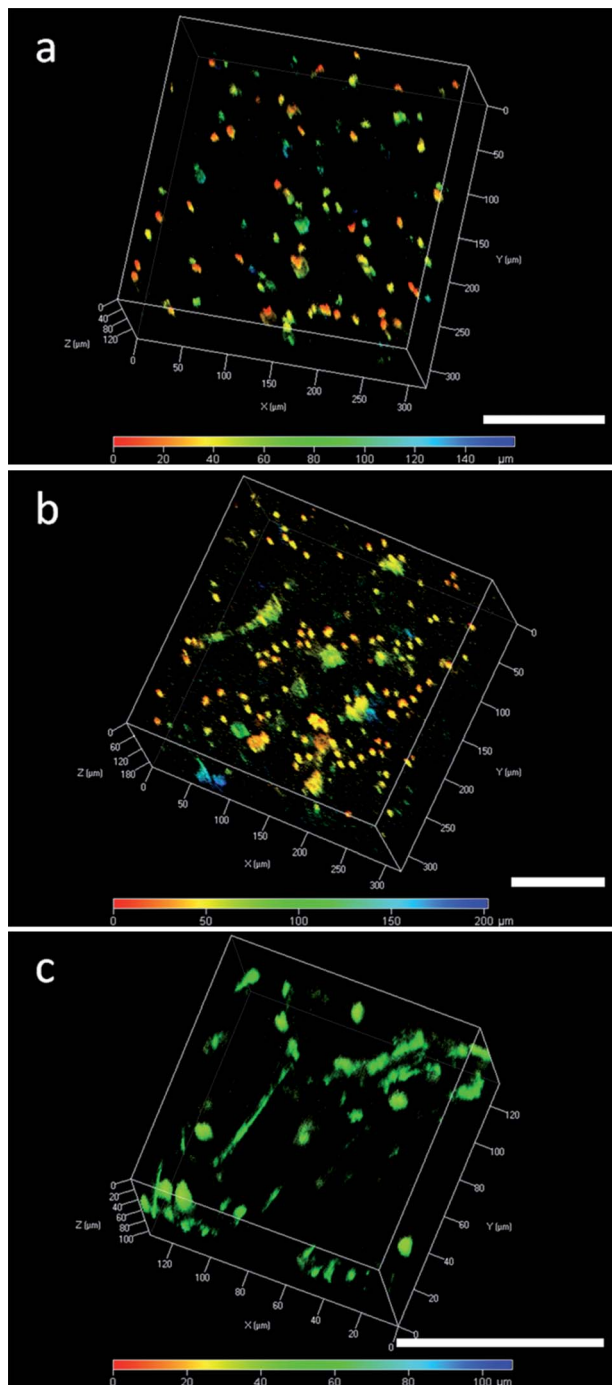


Fig. 11 Detection of the 3D distribution of MC3T3-E1 cells in hydrogels after 4 days of culture. A different color of the cells means they belong to a different layer of the hydrogels. (a) For P hydrogel, (b) for P-D-G-2 hydrogel, and (c) for D-G hydrogel. Fluorescence micrographs were taken by scanning the hydrogels through z axis by using a Laser scanning confocal microscope. Scale bar represents 50 μm .

hydrogel indicates that the cells were almost concentrated on one layer of the hydrogel. This can be attributed to the rapid and uncontrollable degradation of the ODex–MGel hydrogel which made it quickly lose 3D characteristics. However, due to the existence of 4A-PEG-Acr, which is more stable than natural materials, hydrogels of P and P-D-G-2 could keep the 3D structure for a long time. Further evidence of the degradation of hydrogels on day 4 can be obtained from Fig. SI-9.† Additionally, although cells within the P hydrogel can distribute in 3D space, the pure 4A-PEG-Acr component cannot support the spreading and migration of cells. By combining with ODex and MGel, cells spread out easily in the P-D-G-2 hydrogel.

The 3D distribution and spreading of cells within the P-D-G-2 hydrogel was further verified using microscopy photographs (ESI, Fig. SI-10†). When the site was fixed under microscopy sight, through altering the height of the platform slightly, pictures of different heights of the hydrogel can be taken. Cells appearing in different photographs means they belonged to different layers of the hydrogel.

Cell spreading is highly important for obtaining cell–cell contacts, and hence the outcome of tissue.⁴⁹ In a 3D system, cell spreading may be hampered by the physical obstruction of hydrogel networks. It has been proposed that the inclusion of degradable crosslinks sensitive to either hydrolysis⁵⁰ or cell-mediated proteolysis^{51,52} could permit formation of 3D cell extensions, since degradation could generate space for cells to make their way through the matrix, spreading, migrating and establishing cell–cell contacts. In our study, the incorporation of ODex–MGel networks served the dual purpose of providing cells with adhesion sites and allowing degradation to create space for cell spreading and migration. Additionally, the degradation byproducts can also be used to provide nutrition for further tissue regeneration. The 4A-PEG-Acr network can provide cells or tissues with the long-term mechanical and 3D environmental support. Therefore, our two-step IPN hydrogel forming method may be a favorable approach in 3D scaffold fabrication for cell culture.

4. Conclusions

The sequential crosslinking method presented in this study constitutes a simple but powerful technique to fabricate hydrogel scaffolds for 3D cell culture. It was shown that the initial fluid state of this dual crosslinking system was suitable for *in situ* hydrogel-forming applications. The introduction of a light-initiated secondary crosslinking network brought stronger mechanical properties to the IPN hydrogels. Additionally, designing hydrogels from both natural and synthetic polymers also afforded significant control over their degradation behavior. The rapid degradation of IPN hydrogels during the initial days provided space and channels for cells to spread and proliferate, while slow degradation during the later days could provide a long-term 3D environment for cell proliferation. Furthermore, fluorescence micrographs demonstrated that as-prepared IPN hydrogels were cyto-compatible and enabled MC3T3-E1 cells to attach and spread in both 2D and 3D environments. Finally, MTT results demonstrated that the IPN hydrogel provided a favorable 3D environment for MC3T3-E1 cell proliferation. Collectively, our hierarchically designed IPN hydrogel could be a promising injectable scaffold for bone or cartilage regeneration.

Acknowledgements

The authors are grateful to the National Nature Science Foundation of China (project no. 31070871) and Science and Technology Commission of Shanghai Municipality (project no. 11nm0506200) for their support to this project.

Notes and references

- 1 K. Bott, Z. Upton, K. Schrobback, M. Ehrbar, J. A. Hubbell, M. P. Lutolf and S. C. Rizzi, *Biomaterials*, 2010, **31**, 8454–8464.
- 2 M. W. Tibbitt and K. S. Anseth, *Biotechnol. Bioeng.*, 2009, **103**, 655–663.
- 3 K. Y. Lee and D. J. Mooney, *Chem. Rev.*, 2001, **101**, 1869–1879.
- 4 A. Khademhosseini and R. Langer, *Biomaterials*, 2007, **28**, 5087–5092.
- 5 N. Annabi, J. W. Nichol, X. Zhong, C. Ji, S. Koshy, A. Khademhosseini and F. Dehghani, *Tissue Eng., Part B: Rev.*, 2010, **16**, 371–383.
- 6 S. R. Van Tomme, G. Storm and W. E. Hennink, *Int. J. Pharm.*, 2008, **355**, 1–18.
- 7 L. Yu and J. Ding, *Chem. Soc. Rev.*, 2008, **37**, 1473–1481.
- 8 D.-a. Wang, C. G. Williams, Q. Li, B. Sharma and J. H. Elisseeff, *Biomaterials*, 2003, **24**, 3969–3980.
- 9 L. Weng, X. Chen and W. Chen, *Biomacromolecules*, 2007, **8**, 1109–1115.
- 10 L. Weng, H. Pan and W. Chen, *J. Biomed. Mater. Res., Part A*, 2008, **85**, 352–365.
- 11 C. A. DeForest, B. D. Polizzotti and K. S. Anseth, *Nat. Mater.*, 2009, **8**, 659–664.
- 12 C. A. DeForest and K. S. Anseth, *Nat. Chem.*, 2011, **3**, 925–931.
- 13 S. Q. Liu, P. L. Rachel Ee, C. Y. Ke, J. L. Hedrick and Y. Y. Yang, *Biomaterials*, 2009, **30**, 1453–1461.
- 14 M. P. Lutolf and J. A. Hubbell, *Biomacromolecules*, 2003, **4**, 713–722.
- 15 J. Kisiday, M. Jin, B. Kurz, H. Hung, C. Semino, S. Zhang and A. J. Grodzinsky, *Proc. Natl. Acad. Sci. U. S. A.*, 2002, **99**, 9996–10001.
- 16 D. D. Díaz, E. Morin, E. M. Schön, G. Budin, A. Wagner and J. S. Remy, *J. Mater. Chem.*, 2011, **21**, 641–644.
- 17 H. Tan, C. M. Ramirez, N. Miljkovic, H. Li, J. P. Rubin and K. G. Marra, *Biomaterials*, 2009, **30**, 6844–6853.
- 18 R. Jin, L. S. Moreira Teixeira, P. J. Dijkstra, C. A. van Blitterswijk, M. Karperien and J. Feijen, *Biomaterials*, 2010, **31**, 3103–3113.
- 19 R. Jin, L. S. Moreira Teixeira, P. J. Dijkstra, Z. Zhong, C. A. Van Blitterswijk, M. Karperien and J. Feijen, *Tissue Eng., Part A*, 2010, **16**, 2429–2440.
- 20 W. A. Petka, J. L. Harden, K. P. McGrath, D. Wirtz and D. A. Tirrell, *Science*, 1998, **281**, 389–392.
- 21 J. Wu, Z.-G. Su and G.-H. Ma, *Int. J. Pharm.*, 2006, **315**, 1–11.
- 22 J. A. Benton, B. D. Fairbanks and K. S. Anseth, *Biomaterials*, 2009, **30**, 6593–6603.
- 23 A. M. Kloxin, A. M. Kasko, C. N. Salinas and K. S. Anseth, *Science*, 2009, **324**, 59–63.
- 24 J. K. Kutty, E. Cho, J. Soo Lee, N. R. Vyavahare and K. Webb, *Biomaterials*, 2007, **28**, 4928–4938.
- 25 M. D. Brigham, A. Bick, E. Lo, A. Bendali, J. A. Burdick and A. Khademhosseini, *Tissue Eng., Part A*, 2009, **15**, 1645–1653.
- 26 J. Kopeček, *Biomaterials*, 2007, **28**, 5185–5192.
- 27 Y. Liu and M. B. Chan-Park, *Biomaterials*, 2010, **31**, 1158–1170.
- 28 Y. Liu and M. B. Chan-Park, *Biomaterials*, 2009, **30**, 196–207.
- 29 Z. S. Galis and J. J. Khatri, *Circ. Res.*, 2002, **90**, 251–262.
- 30 P. E. Van den Steen, B. Dubois, I. Nelissen, P. M. Rudd, R. A. Dwek and G. Opdenakker, *Crit. Rev. Biochem. Mol. Biol.*, 2002, **37**, 375–536.
- 31 J. A. Burdick and K. S. Anseth, *Biomaterials*, 2002, **23**, 4315–4323.
- 32 T. P. Kraehenbuehl, P. Zammaretti, A. J. Van der Vlies, R. G. Schoenmakers, M. P. Lutolf, M. E. Jaconi and J. A. Hubbell, *Biomaterials*, 2008, **29**, 2757–2766.
- 33 X. Mo, H. Iwata, S. Matsuda and Y. Ikada, *J. Biomater. Sci., Polym. Ed.*, 2000, **11**, 341–351.
- 34 L. Yu, G. Chang, H. Zhang and J. Ding, *J. Polym. Sci., Part A: Polym. Chem.*, 2007, **45**, 1122–1133.
- 35 D. L. Elbert, A. B. Pratt, M. P. Lutolf, S. Halstenberg and J. A. Hubbell, *J. Controlled Release*, 2001, **76**, 11–25.
- 36 M. B. Browning, T. Wilems, M. Hahn and E. Cosgriff-Hernandez, *J. Biomed. Mater. Res., Part A*, 2011, **98**, 268–273.
- 37 C. G. Williams, A. N. Malik, T. K. Kim, P. N. Manson and J. H. Elisseeff, *Biomaterials*, 2005, **26**, 1211–1218.
- 38 W. Xiao, J. He, J. W. Nichol, L. Wang, C. B. Hutson, B. Wang, Y. Du, H. Fan and A. Khademhosseini, *Acta Biomater.*, 2011, **7**, 2384–2393.
- 39 P. Zorlutuna, J. H. Jeong, H. Kong and R. Bashir, *Adv. Funct. Mater.*, 2011, **21**, 3642–3651.
- 40 L. Cai, J. Lu, V. Sheen and S. Wang, *Biomacromolecules*, 2012, **13**, 342–349.
- 41 S. Durmaz and O. Okay, *Polymer*, 2000, **41**, 3693–3704.
- 42 G. H. Altman, F. Diaz, C. Jakuba, T. Calabro, R. L. Horan, J. Chen, H. Lu, J. Richmond and D. L. Kaplan, *Biomaterials*, 2003, **24**, 401–416.
- 43 J. Patterson, R. Siew, S. W. Herring, A. S. P. Lin, R. Guldborg and P. S. Stayton, *Biomaterials*, 2010, **31**, 6772–6781.
- 44 D. Eglin, D. Mortisen and M. Alini, *Soft Matter*, 2009, **5**, 938–947.
- 45 G. M. Kavanagh and S. B. Ross-Murphy, *Prog. Polym. Sci.*, 1998, **23**, 533–562.
- 46 A. K. Gaharwar, S. A. Dammu, J. M. Canter, C.-J. Wu and G. Schmidt, *Biomacromolecules*, 2011, **12**, 1641–1650.
- 47 C.-W. Chang, A. van Spreeuwel, C. Zhang and S. Varghese, *Soft Matter*, 2010, **6**, 5157–5164.
- 48 C. B. Khatriwala, S. R. Peyton and A. J. Putnam, *Am. J. Physiol.: Cell Physiol.*, 2006, **290**, C1640–C1650.
- 49 S. R. Peyton, C. B. Raub, V. P. Keschrums and A. J. Putnam, *Biomaterials*, 2006, **27**, 4881–4893.
- 50 Y. Qiu, J. J. Lim, L. Scott Jr, R. C. Adams, H. T. Bui and J. S. Temenoff, *Acta Biomater.*, 2011, **7**, 959–966.
- 51 J. Sun, W. Xiao, Y. Tang, K. Li and H. Fan, *Soft Matter*, 2012, **8**, 2398–2404.
- 52 T. D. Sargeant, A. P. Desai, S. Banerjee, A. Agawu and J. B. Stopek, *Acta Biomater.*, 2012, **8**, 124–132.